Asymmetric Structural Motions of the Homomeric α7 Nicotinic Receptor Ligand Binding Domain Revealed by Molecular Dynamics Simulation

Richard H. Henchman,* Hai-Long Wang,† Steven M. Sine,† Palmer Taylor,‡ and J. Andrew McCammon*‡
*Howard Hughes Medical Institute, Department of Chemistry and Biochemistry, University of California San Diego, La Jolla, California 92093; †Receptor Biology Laboratory, Department of Physiology and Biophysics, Mayo Foundation, Rochester, Minnesota 55905; and ‡Department of Pharmacology, University of California San Diego, La Jolla, California 92093

ABSTRACT A homology model of the ligand binding domain of the α7 nicotinic receptor is constructed based on the acetylcholine-binding protein crystal structure. This structure is refined in a 10 ns molecular dynamics simulation. The modeled structure proves fairly resilient, with no significant changes at the secondary or tertiary structural levels. The hypothesis that the acetylcholine-binding protein template is in the activated or desensitized state, and the absence of a bound agonist in the simulation suggests that the structure may also be relaxing from this state to the activatable state. Candidate motions that take place involve not only the side chains of residues lining the binding sites, but also the subunit positions that determine the overall shape of the receptor. In particular, two nonadjacent subunits move outward, whereas their partners counterclockwise to them move inward, leading to a marginally wider interface between themselves and an overall asymmetric structure. This in turn affects the binding sites, producing two that are more open and characterized by distinct side-chain conformations of W54 and L118, although motions of the side chains of all residues in every binding site still contribute to a reduction in binding site size, especially the outward motion of W148, which hinders acetylcholine binding. The Cys loop at the membrane interface also displays some flexibility. Although the short simulation timescale is unlikely to sample adequately all the conformational states, the pattern of observed motions suggests how ligand binding may correlate with larger-scale subunit motions that would connect with the transmembrane region that controls the passage of ions. Furthermore, the shape of the asymmetry with binding sites of differing affinity for acetylcholine, characteristic of other nicotinic receptors, may be a natural property of the relaxed, activatable state of α7.

INTRODUCTION

Nicotinic acetylcholine receptors (nAChRs) gate the flow of ions across the membrane of excitable cells in response to agonists such as acetylcholine (ACh). The ligand binding domain (LBD), formed at the interfaces between subunits of the oligomeric nAChR, undergoes a conformational change on binding ACh that triggers opening of the ion channel located in the transmembrane region. Although the structural components and biophysical behavior of nAChRs have been well characterized, the detailed nature of the allosteric sites governing the conformational states remains unresolved (Arias, 1997; Changeux and Edelstein, 1998, 2001; Corringer et al., 2000; Grutter and Changeux, 2001; Sine, 2002; Karlin, 2002; Hogg et al., 2003). The lack of a nAChR structure at atomic resolution has hindered the study of the allosteric mechanism, particularly for modeling methods. The main sources of direct structural information had been the three-dimensional shape of the receptor at 4.6 Å resolution (Miyazawa et al., 1999) and the NMR structure of the M2 helix (Montal and Opella, 2002). Secondary structure determinations had also been derived from the primary sequence (Ortells, 1997; Le Novère et al., 1999). This level of structural data led to simulation studies only of the binding site (Morreale et al., 2002) or the M2 helices in the transmembrane region (Ortells et al., 1997; Tikhonov and Zhorov, 1998; Adcock et al., 2000). However, the recently determined crystal structure of the distantly homologous acetylcholine-binding protein (AChBP) (Brejc et al., 2001) has provided a useful stepping stone forward for such modeling by serving as a suitable template for modeling the nAChR LBD (Le Novère et al., 2002; Schapira et al., 2002; Molles et al., 2002; Sine et al., 2002).

Given the availability of a structure at atomic resolution, molecular dynamics (MD) simulations have proved to be an effective means of determining the structure's dynamic nature, albeit at still very short timescales. In this work, we construct a homology model of the human α7 LBD in a similar manner to that used recently to make a muscle nAChR model (Sine et al., 2002) and examine its stability and dynamic properties in a 10 ns molecular dynamics computer simulation. The α7 nAChR is a suitable choice because it is a homopentamer, the simplest form of nAChR, and its higher sequence identity (Smit et al., 2001) and relatively old ancestry make it a closer mammalian homolog to AChBP, leading to a more reliable model. Physiologically, α7 is widely expressed in the central and peripheral nervous systems and plays a role in many calcium-dependent processes by regulating calcium flow (Hogg et al., 2003).

The MD simulation provides a means to further relax the homology model. Many of the motions seen in the MD simulation would be expected to be optimizations resulting from imperfections in the homology model. The simulation also provides opportunities to observe other types of motion that may correspond with real allosteric motions from the

Submitted May 15, 2003, and accepted for publication August 4, 2003.

Address reprint requests to Richard H. Henchman, 9500 Gilman Dr., Mail Code 0365, La Jolla, CA 92093. Tel.: 858-822-1469; Fax: 858-534-7042; E-mail: rhenchma@mccammon.ucsd.edu.

0006-3495/03/11/3007/12 $2.00

active or desensitized states to the activatable state. Evidence suggests that the AChBP template is equivalent in conformation to the active or desensitized states of the LBD (Grutter and Changeux, 2001). This evidence includes the high affinity of AChBP for nicotinic ligands (Smit et al., 2001) and the closer resemblance to AChBP of the Torpedo nAChR electron microscopy structure with ACh bound than without, the main difference lying in small rotations of the α-subunits (Unwin et al., 2002). With no ligand present in the simulation, the activated or desensitized α7 LBD would be expected to convert into the activatable state. The submicrosecond timescale of MD simulations is still too short to reproduce the full millisecond scale conformational motions. However, even for this short time, by examining the different motions occurring in the ACh binding sites, the Cys loop, and the subunits as a whole, various relationships between these types of motion may be hypothesized.

METHOD

Homology model of the α7 ligand binding domain

We generated a homology model of the LBD of the human neuronal α7 using version 6.0 of the program MODELLER (Šali and Blundell, 1993), together with spatial restraints provided by the AChBP structure (Brejc et al., 2001). The sequence alignment between AChBP and α7 monomers used to generate the homology model is shown in Fig. 1. To maintain complementarity between subunits at their interfaces, all five subunits were modeled simultaneously. The ''patch'' command in MODELLER was used to constrain the coordinates of C127 and C141, which form a disulfide bond in each subunit. The ''refine1 mode'' option was selected to generate the highest level of refinement using conjugate gradients coupled with simulated annealing and molecular dynamics. Modeling included all polar hydrogens to allow for main-chain hydrogen bonding but omitted nonpolar hydrogens. In this way, 100 different structures were produced and evaluated using the programs PROCHECK (Laskowski et al., 1993) and PROFILES-3D in InsightII. The majority of the 100 structures scored high in these evaluations, and we chose the one that ranked highest by PROCHECK. Unlike our previous modeling of the human muscle nAChR (Sine et al., 2002), the linkers between β-strands 8 and 9 required no further modeling due to a gap of only three residues in the sequence of α7 rather than an insertion of 8–11 residues in muscle nAChR. Two rounds of energy minimization were applied using the program CHARMM (Brooks et al., 1983), version 27b4. The first round constrained the coordinates of all heavy atoms while allowing mobility of all hydrogens. The second round constrained the protein main chain while allowing mobility of all the side chains. In the next stage, the protonation states of all titratable residues and orientation of asparagine and glutamine amide side chains were determined using the WHAT IF program including optimization of the hydrogen bond network (Vriend, 1990). Standard protonation states were found for all residues. The position of the ionizable proton on histidine was $N_{\delta 1}$ for H114 and $N_{\varepsilon 2}$ for H62, H104, and H140. The LBD alone numbers 16,835 atoms. Water oxygen atoms were placed close to the LBD using the GRID program (Goodford, 1985) with an energy cutoff of -8 kcal/mol^{-1} and otherwise default parameters. This added 552 waters. Hydrogens were added to the LBD and the water oxygen atoms so as to optimize the hydrogen bond network using the WHAT IF program (Vriend, 1990). The resulting system was solvated in a 100 Å cubic periodic box using the ''tleap'' module of AMBER 7 (Pearlman et al., 1995). Finally, 74 Na^+ and 54 Cl^- ions were randomly swapped with single water molecules, one each, to produce a neutral system and mimic 0.15 M and 0.11 M concentrations for Na^+ and Cl^- ions. None of the added ions was buried in the LBD. The total number of resulting water molecules was 27,248.

MD protocol

Further minimization and MD were carried out using the ''sander'' module of AMBER 7 (Pearlman et al., 1995). The system was modeled with the AMBER parm99 force field (Wang et al., 2000) and TIP3P water (Jorgensen et al., 1983). Nonbonded interactions were calculated up to a cutoff of 9 Å with particle mesh Ewald (Essmann et al., 1995) for long-range interactions. The whole system was first minimized for 200 steps using the steepest descent algorithm to remove bad contacts. A short 5 ps molecular dynamics simulation at 50 K and constant volume equilibrated the solvent with the LBD fixed. The whole system was then gradually warmed up to 300 K in six simulations of 5 ps at 50 K intervals at constant pressure (1 atm) then extended to 10 ns at 300 K. All dynamics simulations were run with SHAKE (Ryckaert et al., 1977) and a 2-fs time step. A Berendsen thermostat and barostat with isotropic scaling (Berendsen et al., 1984) maintained temperature and pressure. The coupling time was 1 ps for the thermostat, 0.1 ps for the barostat during equilibration, and 1 ps for the barostat afterward. The equilibration phase was run on a dual processor Alpha EV67 and the remainder on Blue Horizon at the San Diego Supercomputer Center.

ACh docking

ACh was docked to each binding site in snapshots selected from the MD simulation to assess how intact the binding site remained during the simulation. ACh was optimized in the extended conformation using Gaussian 98 (HF/6-31G*) and parameterized with Gasteiger-Marsili charges (Gasteiger and Marsili, 1980), which use the united atom representation for nonpolar hydrogens. With all four of its dihedrals flexible, ACh was docked to each binding site in snapshots taken every 10 ps using the AutoDock 3.0.5 program (Morris et al., 1998). A standard docking protocol with default parameters and the Lamarckian genetic algorithm was used, with the following exceptions. To achieve a more thorough search, the initial population size was set to 200, and 50 independent runs were performed per binding site on a 30 Å cubic grid centered on the atom C189:S_γ with grid spacing 0.375 Å. The positions of the nitrogen and carbonyl carbon atoms of ACh from the 50,000 docked positions at each binding site were placed on a 30 Å cubic grid of spacing 1 Å. This relatively large grid makes docking possible outside the binding site.

```
          1        10        20        30        40        50        60        70
α7:       EFQRKLYKELVKNYNPLERPVANDSQPLTVYFSLSLLQIMDVDEKNQVLTTNIWLQMSWTDHYLQWNVSE
AChBP:    FDRADILYNIRQTSRPDVIPTQRD-RPVAVSVSLKFINILEVNEITNEVDVVFWQQTTWSDRTLAWNSSH

          71        80        90        100       110       120       130       140
α7:       YPGVKTVRFPDGQIWKPDILLYNSADERFDATFHTNVLVNSSGHCQYLPPGIFKSSCYIDVRWFPFDVQH
AChBP:    S--PDQVSVPISSLWVPDLAAYN-AISKPEVLTPQLARVVSDGEVLYMPSIRQRFSCDVSGVDTESG-AT

          141       150       160       170       180       190       200
α7:       CKLKFGSWSYGGWSLDLQMQEA---DISGYIPNGEWDLVGIPGKRSERFYECCKEPYPDVTFTVTMRRRT
AChBP:    CRIKIGSWTHHSREISVDPTTENSDDSEYFSQYSRFEILDVTQKKNSVTYSCCPEAYEDVEVSLNFRKKG
```

FIGURE 1 Alignment between the LBD of α7 and AChBP. Numbering is for α7.

RESULTS

The following color scheme and notation are used to clarify the correlations among the five homomeric subunits as they diverge from a structure with a fivefold axis of symmetry. The subunits are labeled S_A, S_B, S_C, S_D, and S_E in a counterclockwise direction as viewed from the N-terminus looking down through the pore, and colored yellow, orange, red, magenta, and purple, respectively. The subunit at the clockwise side of each interface as viewed from the N-terminus is called ''plus'', and the other ''minus.'' Interfaces between the pairs of subunits are labeled I_{AB}, I_{BC}, I_{CD}, I_{DE}, and I_{EA}, where the letters refer to the plus and minus subunits.

Homology model

Homology models for $\alpha 7$ have already been published by Schapira et al. (2002) and Le Novère et al. (2002) for the very similar chick instead of the human. The alignment of Schapira and co-workers is quite different from ours regarding the position of gaps and insertions. Given that our alignment is backed up by the lysine scanning mutagenesis technique (Sine et al., 2002), we have greater confidence in the alignment used here. Regarding the other published homology model, the alignment and, consequently, backbone of our human $\alpha 7$ model is almost identical with the chick $\alpha 7$ model of Le Novère and co-workers. A trivial difference is the residue numbering. The numbering differs by one because Le Novère et al. omit E1, present in our model, such that F2 in our numbering is F1 in theirs. The more significant difference is in the alignment from residues E1 to P15, which is shifted one residue lower in their structure such that their residue F2 matches our residue E1 up to their K11 matching our V12. The alignment by Le Novère and co-workers gains sequence identity at L6 and K7 at the cost of an extra insertion in $\alpha 7$. Which alignment is better is uncertain, given the low sequence identity in this region. The backbones superimpose identically except with small deviations at loops 12-15, 24-26, 72-74, 94, 138-139, 162-165, and 169-170. There is quite a bit of variation in the side-chain placing throughout the model, though the binding-site side chains are very similar. The nearest side chains to the binding site that differ substantially in position are those of N52 and Y167.

Energetic stability

The LBD's potential energy and potential energy components, smoothed over 100-ps intervals, are presented in Fig. 2 for the duration of the simulation. The potential energy during the 30-ps warming-up stage has been omitted. The behavior of the potential energy is characteristic of having a homology model as the starting structure. After an initial large relaxation, the potential energy continues to decrease more sporadically. Excluding the initial relaxation in the minimization and the warming-up stage, there is a total

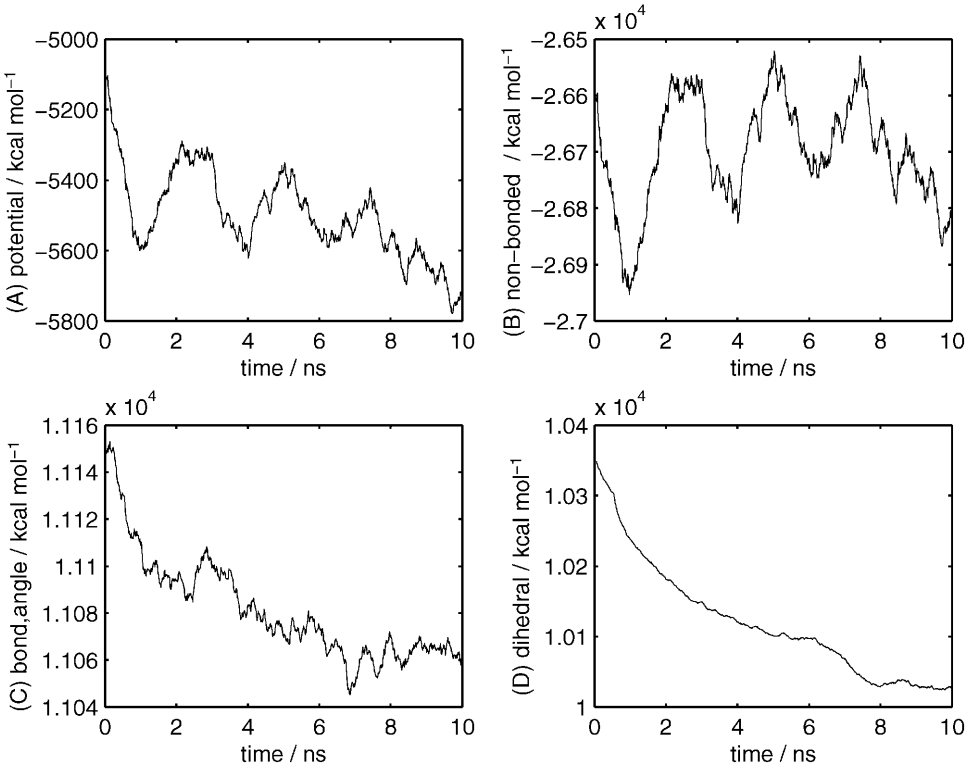

FIGURE 2 (*A*) The potential energy of the LBD (excluding solvent) during the molecular dynamics simulation. The components of the potential energy are (*B*) nonbonded energy, (*C*) bond and angle energy, and (*D*) dihedral energy.

decrease of 600 kcal/mol^{-1} in the LBD. This change translates to 0.06 k_BT per atom, still a small fraction of the thermal energy, 3/2 k_BT. Approximately half of the relaxation comes from the dihedral term, a third from the nonbonded term, and a sixth from the bond/angle term. Unlike the other two terms, the nonbonded term fluctuates quite substantially, presumably because this term, unlike the others, contains interactions with the solvent. If the solvent is included, the energy of the whole system including solvent (not shown) appears to have leveled off after 8 ns. Overall, 10 ns of simulation leads to a reasonable improvement in energy. It is unlikely that the final structure represents the activatable state after this relatively short time. A much longer simulation of probably impractical length at this stage would be required to fully relax the structure to that point.

Structural stability

The root mean-squared deviation (RMSD) provides a means of evaluating how much the structure deviates from the starting homology model during the simulation. Fig. 3 *A* shows the RMSD of all C_αs in each subunit and the average relative to the homology model, smoothed over 500-ps intervals to improve readability. The RMSD is calculated after superimposing each frame of the whole LBD on the starting homology model. The colored lines are the RMSD

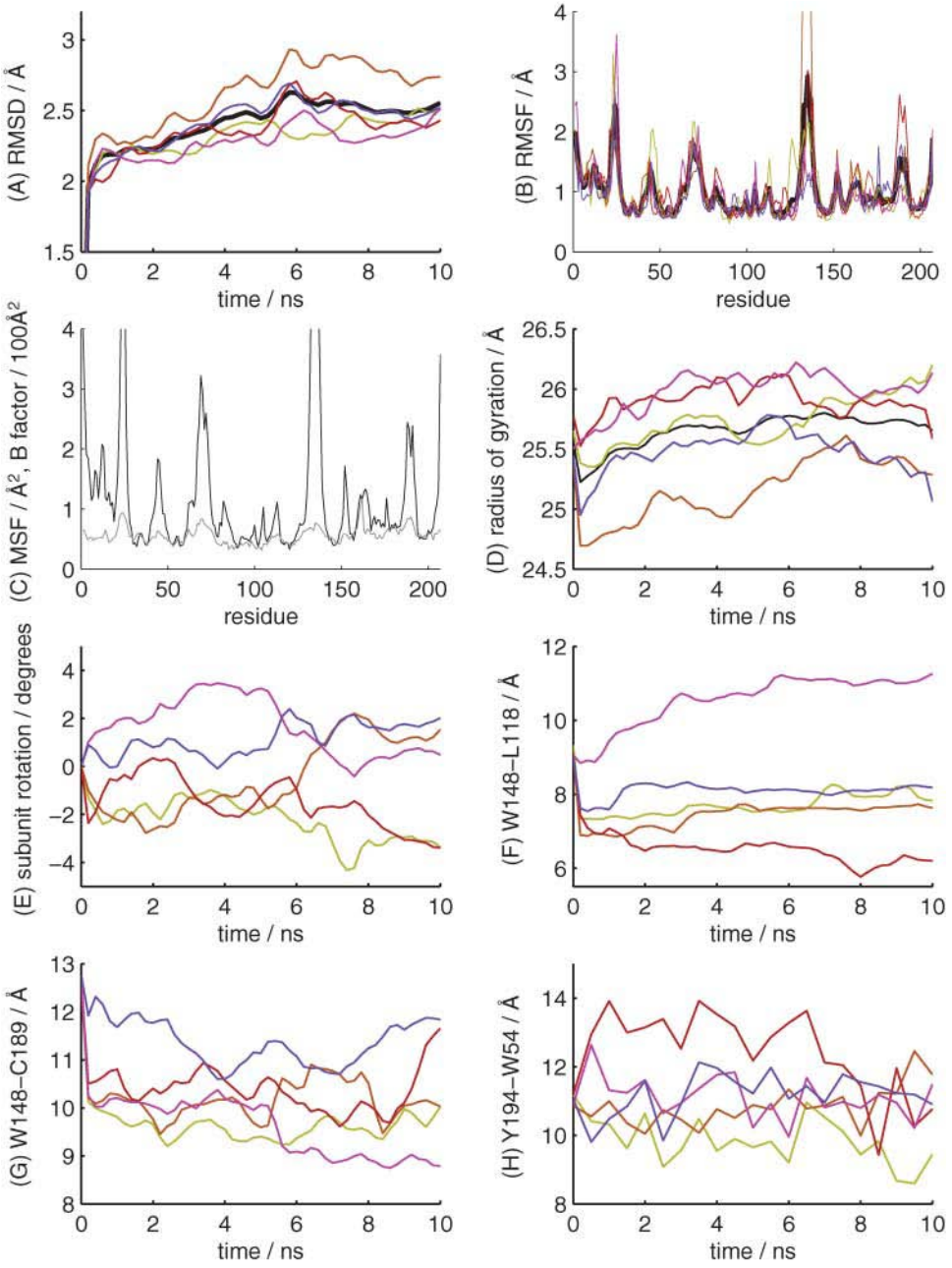

FIGURE 3 Structural data of the LBD from the molecular dynamics simulation. The color represents each subunit. Subunits S_A–S_E are colored yellow, orange, red, magenta, and purple. The average of all five subunits is black, whereas experimental B-factors are gray. All information is calculated using C_α atoms. Time series data are smoothed over 500 ps intervals. (*A*) RMSD relative to the initial structure. (*B*) RMSF relative to average structure. (*C*) MSF averaged over the five subunits versus B-factors for AChBP (Brejc et al., 2001), using the alignment in Fig. 1. (*D*) Radius of gyration relative to the center axis of the whole LBD. (*E*) Rotation of each subunit around an axis through its center and parallel to the pore. (*F–H*) Three distances important in defining the shape of the binding site are W148–L118, W148–C189, and Y194–W54 (L118 and W54 are on the minus side of the subunit interface). The distances are defined between the C_α atoms of each residue. The color refers to the plus interface.

for each subunit and the black line is the average over all five subunits. The RMSD increases rapidly at first due to thermal vibrations and relief of unoptimized interactions in the homology model. At ~2.5 Å, the RMSD levels off a moderate amount. All subunits behave similarly with the exception of S_B, which has a larger RMSD, the reason for which is apparent in the next section. Although it is not known at this stage how close the homology model is to the real $\alpha 7$ structure, this relatively stable behavior of RMSD further supports the homology model as a plausible structure.

Residue mobility

More specific information on different residue mobility is provided by the root mean-square fluctuation (RMSF) relative to the average structure. The average structure was created by superimposing each frame every 1 ps on the starting frame and taking an average. The RMSF of each C_α, also from each frame every 1 ps, is illustrated in Fig. 3 *B*. Mapping the RMSF onto the subunit structure in Fig. 4 and coloring according to value shows where the mobility lies. Blue is least mobile, green intermediate, and red the most mobile. Overall, the structure is very stable, particularly the β-strand regions colored blue with RMSF <1 Å. This stability is encouraging for the homology model. Excluding the chain termini, mobile parts are the helix 3-13 and the loops 23-25, 43-46, 62-74, 130-139 (Cys loop), 152-153 (loop B), 160-166 (loop G), and 186-193 (loop C). This pattern of RMSF for all five subunits is reasonably consistent among themselves and with the experimental B-factors of AChBP (Brejc et al., 2001) plotted in Fig. 3 *C*. Here, the MSF (mean-square fluctuation) rather than the RMSF is plotted for consistency with the B-factors. B-factors, shown in gray and scaled by 100, are plotted using the alignment in Fig. 1. The simulation of the $\alpha 7$ model displays flexibility in the expected places and the secondary structure remains constant and intact for the duration of the simulation. Of the seven loops that contribute to the ligand binding site, loops B, C, and (to a lesser extent) G are more flexible, whereas A, D, and F are fairly rigid. The most flexible loop is the Cys loop at the base of the LBD that most probably interacts with the transmembrane region between the M2 and M3 helices. In S_B, this loop moves by as much as 7 Å toward the right as drawn in Fig. 5. The new loop position is stabilized by a salt bridge between R132 on the Cys loop and E44 on the same subunit. This motion contributes substantially toward the increase in RMSD for S_B (Fig. 3 *A*). However, this same salt bridge still forms for three other subunits, S_A, S_D, and S_E, although with less contact. The implications of this will be discussed later.

Subunit motion

Motion may also occur on the level of the subunits and the whole LBD. Even though the 10-ns simulation is short relative to the timescale of receptor activation, the LBD does exhibit some subunit motion during this time. The radius of gyration, R_g, calculated in the plane of the LBD perpendicular to the pore axis, measures the breathing of the pore and is defined as:

$$R_g = \left(\sum_i m_i r_i^2 / \sum_i m_i \right)^{1/2},$$

where the sum is over C_α atoms, m_i is the mass of the atom, and $r_i = (x^2 + y^2)^{1/2}$ is the distance of the atom from the central axis of the receptor (the z axis). Fig. 3 *D* shows how R_g of the whole LBD changes (in *black*) during the simulation, smoothed over 500-ps intervals. After an initial

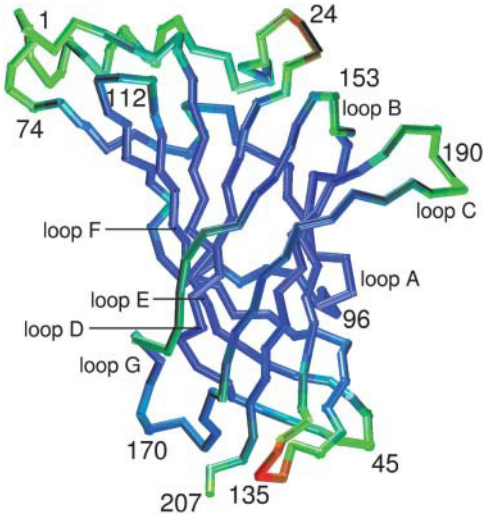

FIGURE 4 RMSF of each residue averaged over the five subunits mapped onto the structure of the LBD (*red* is the most mobile; *blue* is the least). The figure was made using the program VMD (Humphrey et al., 1996) and rendered with Raster3D (Merritt and Bacon, 1997).

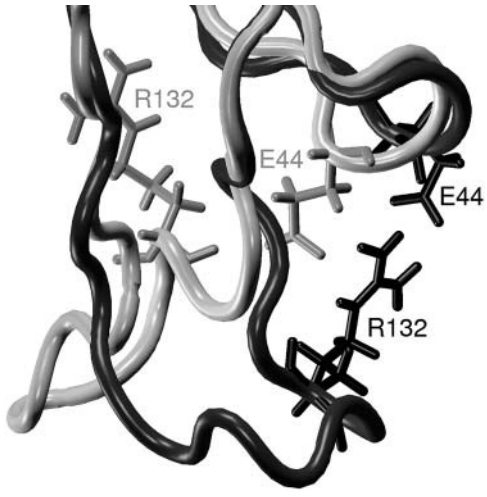

FIGURE 5 The motion of the Cys loop in S_B from the homology model (*white*) to after 10 ns (*black*). The formation of the salt bridge between R132 on the Cys loop and E44 after 10 ns is also indicated.

sharp drop from 25.5 Å, the LBD undergoes a gradual expansion by 0.5 Å, followed by a slight contraction toward the end. This slight expansion may arise from a number of causes. It may be relief from the confinement of crystal packing; it may result from suboptimal packing in the homology model; or it may represent natural motion of the LBD, showing that it is capable of breathing.

This breathing motion may be more precisely interpreted by breaking it down into contributions from each subunit. Fig. 3 *D* also shows R_g for each subunit about the same LBD axis, smoothed by 500 ps. Two subunits, S_B and S_E, are responsible for the initial drop in total R_g seen earlier. All five subunits then expand outward slowly before contracting slightly toward the end. After 10 ns, relative to the homology model, two subunits, S_B and S_E, have shifted inward; S_A and S_D have moved outward, whereas S_C ends up close to the average. These motions lead to a slightly distorted, asymmetric structure. The sizes of these motions are small, ranging from ~0.6 Å for S_A, S_B, and S_C to ~1.0 Å for S_D and S_E. These motions are depicted in Fig. 6, which shows the structures of the model and after 10 ns. For the model structure, the large, straight arrows indicate the motion that the center of mass (C_α atoms) of each subunit undergoes to move to the 10-ns structure. Likewise, the arrows on the 10-ns structure indicate how the subunits would move to return to the model structure and, correspondingly, are the reverse of those shown for the model structure. The smaller arrows represent the same motion at a finer level averaged over triplets of consecutive C_αs. The large arrows are consistent with the values of R_g.

As well as translation, the subunits also undergo slight rotations by a few degrees, shown in Fig. 3 *E* and smoothed over 500-ps intervals, and in Fig. 6 by the curved arrows. Rotation of each subunit is defined about the axis passing through its respective center of mass and parallel to the pore. The angle represents how far the subunit has rotated relative to its starting orientation. Counterclockwise is the positive direction. S_A and S_C gradually twist clockwise during the simulation, while S_E moves counterclockwise. S_B twists slightly clockwise, then reverses to counterclockwise, whereas S_D initially deviates counterclockwise but finishes close to its starting value. These rotational motions are reasonably consistent with the translational motions of the adjacent subunits. For example, the clockwise motion of S_C is matched by an inward motion of S_B and an outward motion of S_D. Not all of the observed motion is purely radial. In particular, S_D marginally separates from S_E and S_A less so from S_B, whereas S_C and S_D come together, as do S_E and S_A. Parallel to the pore axis, the only significant but still small motion is a slight upward movement of S_B and a downward movement of S_C.

These different subunit motions would be expected to have an effect on their intersubunit interfaces and, consequently, the binding sites. A number of different types of interface should arise. I_{AB} and I_{DE} both involve a shear motion of the plus subunit moving out relative to the minus subunit and a slight separation due to the outward movement of S_D and S_A. I_{BC} remains reasonably stable between two subunits moving inward together. I_{CD} and I_{EA} undergo compression due to the slight radially inward motion of the plus subunit. They also undergo a shear motion this time, with the plus subunit moving inward relative to the minus side. How these expected movements are borne out in the binding sites is examined in the next section.

Binding site changes

A range of different behavior is found for each of the five binding sites. Fig. 7 depicts the binding site motions at all five interfaces. Each row represents one binding site as viewed from the side with the plus side on the left and the minus side on the right. The identity of the participating subunits is indicated by the colored letters. On each row, the two structures on the left are the binding site residues of the model and after 10 ns. Shown are residues Y92, W148, Y194, and C190 on the plus side, and W54 and L118 on the minus side. Two other important residues making up the binding site, Y187 and C189, both on the plus side, are omitted for clarity and behave similarly to C190. The arrows, here marked in green, point in the direction that the C_α atoms of these residues move to go from the current structure to the

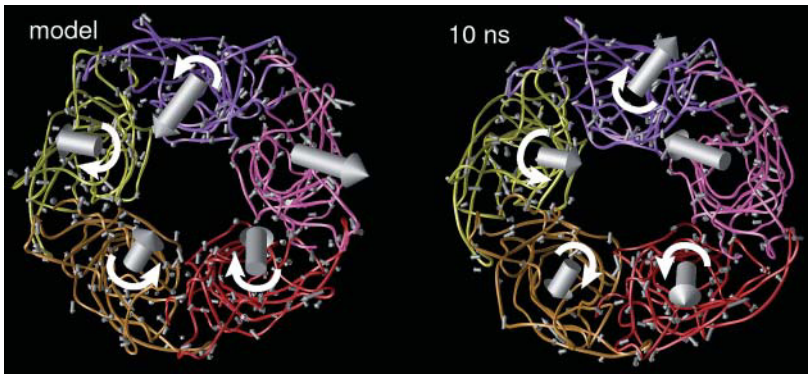

FIGURE 6 Changes in the structure of the LBD between the model and the end (10 ns) of the simulation as viewed from the N-terminus. Subunits S_A–S_E are colored yellow, orange, red, magenta, and purple. The direction the subunit translates (*large straight arrows*) and the direction the subunit rotates to get from one structure to the other (*large curved arrows*) are indicated. The arrows describing the translations are to scale, whereas those describing the rotations are not. The rotation arrow for S_D is omitted due to its small size. The small arrows represent the translational information at a finer level of detail, averaged over triplets of residues (triplets are chosen to aid visibility). Structures were made with OpenDX using the chemistry modules (Gillilan and Wood, 1995).

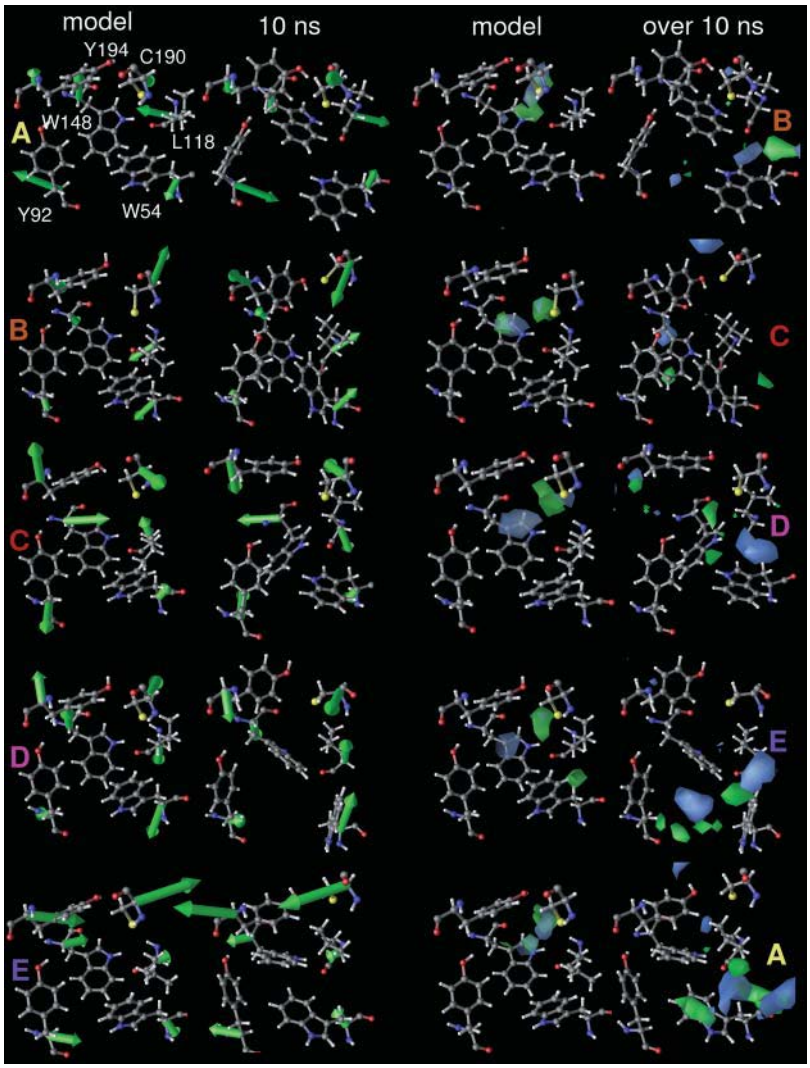

FIGURE 7 Changes in the structure of all five binding sites. Each row represents the binding site at each interface. The two colored letters identify the left and right subunits that form the interface. Starting from the left, the first structure is the starting structure for each binding site, and the second is the final structure after 10 ns. The direction is shown in which each residue's C_α moves to go from that particular structure to the other structure (*green arrows*). The third structure shows the docking results of ACh to each binding site of the starting homology model. The third structure shows the docking results of ACh to each binding site of snapshots every 10 ps in the simulation. Regions are shown representing where the ACh's N and carbonyl C atoms, respectively, cluster (*blue* and *green*). The fourth structure is docking of ACh to multiple snapshots every 10 ps over the entire simulation. Structures were made with OpenDX, using the chemistry modules (Gillilan and Wood, 1995).

other structure. The third and fourth structures in each row show the result of ACh docking, to be discussed later.

The motion of the binding site C_α atoms is generally consistent with the global subunit motion, supporting the premise that the subunit motion occurs in real nAChRs rather than being simply the artifact of an internal localized motion. At I_{AB} and I_{DE}, residues on the plus side move out whereas those on the minus side move in—the same shear motion seen earlier. All residues at I_{BC} move inward as do S_B and S_C. Some compression is seen at I_{CD} and I_{EA}, although the shear motion with the plus side moving inward relative to the minus appears to be absent. The interfaces appear unable to shear in this direction. At the I_{CD} interface, all the residues move outward. Even though S_C moves in slightly, it also rotates clockwise, explaining the outward motion at this interface. The main motion at I_{EA} is a shift of both subunits counterclockwise and some compression of the binding site residues. The clockwise rotation of S_A offsets its outward motion at I_{EA}, leading to little net radial motion at this interface.

The time series of these motions may be seen in a selection of distance plots in Fig. 3, *F–H*, smoothed by 500 ps. The color refers to the plus subunit at the interface. The following distances are defined between the C_α atoms of the following residue pairs. The W148–L118 distance captures the width of the binding site between the two subunits. Starting at 9 Å, this distance decreases for four of the five interfaces, especially at I_{CD}. The drop at the start is quite rapid. I_{DE} is the exception where shearing and slight separation take place. How the atoms move to alter these distances may be seen from the arrows on these residues in Fig. 7. A particularly conspicuous motion in the binding site is the inward movement of loop C containing Y187, C189, and C190 into the binding site. The C_α distance, W148–C189, plotted in Fig. 3 *G*, decreases by 2–4 Å at I_{AB}, I_{BC}, and I_{DE}, and less so at I_{CD} and I_{EA}. Residues Y187, C189, and C190 move fairly concertedly, and all their distances with W148 behave similarly for each interface. The decreased contraction of loop C at I_{CD} and I_{EA} may be explained by the shear

motion described earlier whereby the minus subunits, S_D and S_A, move outward (Fig. 6) to counteract loop C. The fluctuation of this distance is quite large and is due to the mobility of loop C, also evident in its greater flexibility in the RMSF (Figs. 3 *B* and 4) and the larger arrows of C190 in Fig. 7. The backbone of W148, the other atom defining this distance, is much more stable. One final distance that differs significantly among subunits is Y194–W54, which loosely measures the height of the binding site. This increases at I_{DE} due to the shearing and separation, and at I_{CD} for which Y194 moves upward and marginally at I_{AB}, mentioned earlier, yet contracts at I_{BC} and I_{EA}. As well as distances that change, some other clusters of residues remain more together and are separated by fairly constant distances (not shown). One unit is Y92, W148, and Y194, with the exception of I_{CD} in which Y194 moves upward away from the other two. Another such unit is W54 and L118, which are also separated by a fairly constant distance. A third unit is Y187, C189, and C190. Interestingly, Y92 also remains relatively fixed with respect to W54 and L118 across the interface, whereas W148 does not. Y92 also remains fairly fixed with respect to Y187, except early on in S_C. Hence, Y92 appears to act as an intermediary between W148 and W54. This behavior is consistent with the proximity of each residue's side chain.

The side chains of the binding site residues display a few notable differences after 10 ns. The most striking is the crowding of the binding site. Starting from a relatively open site, the side chains move in to partially fill the site. Three residues possess side chains that differ markedly between interfaces: W54, W148, and L118. The chief residue responsible for the shrinking is W148. In all cases but I_{BC}, the lower half of the W148 indole ring swings into the site. A small dihedral change is sufficient to bring this about and does not involve a complete transition between rotameric states, as both side-chain dihedrals, χ_1 and χ_2, remain *gauche*+ and *gauche*−, respectively. A larger change is seen at I_{CD}, for which χ_1 of W148 goes from *gauche*+ to *trans*, twisting the indole ring to the side in response to the collapsing binding site. At the other extreme, the W148 indole ring at I_{BC} remains fixed in place because W54 swings up and blocks it from doing so. This other tryptophan, W54, also undergoes quite different behavior at each interface. Most of the difference lies in χ_2. At I_{AB}, I_{CD}, and I_{DE}, χ_2 remains *gauche*− and twists down the indole ring slightly, opening up the entrance to the binding site. However, at I_{BC} and I_{EA}, χ_2 swings up the ring to become *gauche*+, further crowding the binding site. In the case of I_{EA}, W54 even manages to get behind W148, further raising that residue. Coincidentally, both of these interfaces are ones that are compressed. I_{DE} is the only interface where χ_1 of W54 also changes, going from *trans* to *gauche*−, pulling the indole ring farther from the site. L118 is the third residue whose side-chain dihedrals differ among interfaces. One notable feature about this residue was that during the first stages of minimization, its side chain in each subunit adopted different conformations. In particular, χ_1 is *trans* at I_{AB} and I_{DE}, and *gauche*+ for the other three interfaces. During the simulation, both χ_1 and χ_2 largely remain *gauche*− in I_{BC} and I_{EA}, both *trans* in I_{AB} and I_{CD}, and respectively *gauche*− and *trans* in I_{DE}. The *trans* position of χ_1 keeps the side chain more out of the binding site, whereas the *gauche* conformations point it in. Most of the other side chains in the binding site remain fairly constant in conformation. Their only major fluctuations are for Y92 in I_{AB} between *trans* and *gauche*− and C189 and C190 in I_{BC}. The occasional tyrosine ring flips also occur.

ACh docking

The results of docking ACh to each binding site are illustrated in the third and fourth columns of Fig. 7. The residue positions are those of the homology model and after 10 ns. Green regions show where the ACh's carbonyl carbon docks, and blue regions where the nitrogen docks. More specifically, each colored region is an isocontour with one docking hit per grid cube (1 $Å^3$) for docking to the starting model, and 250 hits per grid cube for docking to the snapshots. With 50 docking runs per snapshot and 1000 snapshots, 50,000 docking conformations were generated per binding site. What is abundantly clear is that, whereas it docks well to the homology model, ACh docks poorly to the binding site for most of the structures generated by the simulation. For the starting structure, the docked positions are very similar to the docking of ACh to α7 by Le Novère et al. (2002). This is the site in which the HEPES buffer molecule lies in the AChBP crystal structure (Brejc et al., 2001). The choline end of ACh lies at the middle of the W148 indole ring nestled between the other aromatic side chains of W54 and Y92. The acetyl end of ACh lies near the top of the W148 indole ring and is bounded by N106, V107, L108, and Q116 (these residues omitted from the figures for clarity). The choline group makes cation-π interactions with the aromatic groups; the acetate methyl group lies in a hydrophobic cleft, whereas the carbonyl oxygen forms a hydrogen bond either with the backbone amide hydrogen of L118 or the polar $H_{\varepsilon 1}$ of W148. In the case of some interfaces, particularly I_{AB} and I_{EA}, the orientation of ACh flips by 180°. This probably arises either from a force-field deficiency, particularly in the cation-π interaction, or is characteristic of the homology model.

The docking positions for the homology model are not seen in the docking results for the whole simulation since they fail to occur often enough to surpass the 250-hit threshold. Rather, docking positions predominate elsewhere. The most common cluster is on the face of W54 as it swings away from the binding site, present in all cases except I_{BC}. Apart from a smattering of clusters on the LBD surface, two other interesting binding sites are observed. One lies in I_{DE} below the W148 indole ring. At this interface occurs the shearing motion and slight separation of the two subunits. The outward motion of W54 and the extra space due to the

interface separation contribute to increasing the space that ACh occupies. The other site lies in I_{BC} behind W148 instead of in front. This is the interface for which the W148 indole ring remains relatively stationary and S_B and S_C move inward in concert. This site opens up due to the motion of the ring of F103 on the minus interface early on in the simulation that blocks this site in the other interfaces. F103 itself backs onto an indentation in the inner pore. Thus a total of four binding sites are observed including the initial one. Assuming that the site preferred in the model is the actual ACh binding site in the ligand-bound state, the side chains that move during the simulation to overlap with ACh in this position would be those that have to move aside for ACh to bind and activate the receptor. The principal residues that sterically overlap with ACh in its preferred docked position in the model are W148 and L118 (the most followed by the three tyrosines); Y194, Y187, Y92; and C189, and C190 on loop C, with W54 only clashing at I_{BC} and less so at I_{EA}.

DISCUSSION

A molecular dynamics simulation has been run for 10 ns on a homology model of the LBD of α7 based on the AChBP crystal structure to test the validity of the structure. Ideally, the simulation would be started from a crystal structure of α7 but given the current absence of knowledge of such a structure, a homology model is the next best alternative if any modeling work at the molecular level is to be attempted. The simulation leads to a large reduction in the energy of the homology model, producing an improved, more relaxed, structure. The overall structure of the LBD remains fairly constant during this relaxation at the secondary and tertiary levels of structure, supporting the validity of the initial model. The RMSF only increases to a moderate value, and what backbone flexibility is seen in the crystal structure B-factors, predominantly loop motion, is also seen in the simulation MSF. Much of the remaining relaxation is due to small atom rearrangements and side-chain repacking, an aspect not examined in this work except in the binding site. The accuracy of the model is expected to be greater in the binding site given the greater sequence identity between α7 and AChBP. Based on the continually decreasing trend in energy, 10 ns appears insufficient to fully relax the model, yet it is still adequate to assess the model quality and to glean some information on the flexibility of the LBD.

Studying the LBD flexibility is the other purpose of this investigation. α7 has pentameric symmetry, and over a long enough time, each subunit might be expected to experience the same types of motion. However, because molecular motion is stochastic and the simulation time is short, each subunit will undergo different motions during the simulation. Furthermore, by observing the types of motion occurring in the LBD and exploiting the different patterns of motion seen in different subunits, insight is gained into how motions in the binding site in response to ligand binding might correlate with other motions elsewhere that connect to the ion channel in the transmembrane region. The analysis of the simulation reveals three types of motion taking place. These are motions of the side chains in the binding site, loops, and whole subunits. Motion can arise from a number of sources. It may either be a consequence of going from the crystalline to the liquid phase, relaxation of the homology model, relaxation to the closed state, the force field, absence of the transmembrane region and lipid bilayer, or random noise due to flexibility in the structure. It is difficult at this stage, given the homology model and the short timescale, to be certain of the nature of each type of motion.

The foremost motions relevant to ligand binding are those taking place in the binding site. The main result observed here in the simulation is the shrinking of the binding site dimensions. The principal contributions to this process are the swinging in of the W148 indole ring, the inward motion of loop C, and the decrease in separation between the backbones of the Y92/Y194/W148 and W54/L118 units. Less important contributions to shrinking come from the Y92, Y187, Y194, and L118 side chains. The contribution of these three tyrosines-to-agonist binding has been noted in mutagenesis studies (Sine et al., 1994). W54 more commonly swings away from the binding site, but it may move in as well in the cases of I_{BC} and I_{EA}. There is strong evidence for the importance of W148 and W54 to ligand binding (Corringer et al., 1995; Zhong et al., 1998), and the different conformations of these residues among binding sites observed in the simulation suggests that they have some flexibility. The second contribution to binding site shrinkage is the inward motion of loop C.

The absence of a ligand creates space, allowing the loop to move in. The final contribution, the distance between residue backbones at the interface, appears to be correlated with subunit motion, discussed below. The trend here is not so uniform. I_{BC}, I_{CD}, and I_{EA} display slight compression whereas I_{AB} and I_{DE} are more open. The sum effect of these three contributions still leads to shrinking of the binding site for all five cases. This shrinking all but prevents ACh from docking as would be expected in the crystal structure. Consequently, ACh prefers to dock elsewhere, either over W54, or under or behind W148. This docking site behind W148 is rather speculative. It arises due to a displacement of the F105 side chain, forming a cavity there. ACh may reach this position if it is able to burrow under W148 as it does when docking to I_{DE}. Overall, when ACh is present in the simulation, it would presumably encourage expanding motions of the binding site to enter the site. Although the side chains and loop C appear to encroach on the binding site, their flexibility suggests that they would not act as too large an obstacle for the entrance of ACh. Their displacement upon ACh binding may even contribute to the resulting conformational change. On the other hand, the motions may be a result of imperfect side-chain packing in the homology model or inadequate solvation of the binding pocket in the

initial setup. The use of GRID to place waters and some solvent-only equilibration lead to partially solvated binding sites, although the actual extent of hydration of the largely hydrophobic binding sites remains unknown. If these binding site motions are realistic, then it adds further weight to the idea that the homology model of α7 and AChBP are in the ligand-bound state, for ACh binding would only be favored when the binding site is open.

It is not known by what mechanism ligand binding induces the opening of the transmembrane pore. Based on the flexibility observed in the simulation, one possible means is via subunit motions. It should be noted that modeling the subunit motions as translations and rotations is only approximate. Subunits also have more complex and subtle internal motions that indirectly contribute to translational and rotational motion, although no clearly characterizable flexibility at an intermediate level such as within the β-strands was identified here. Nevertheless, this analysis still serves as a useful tool to dissect motion. The whole pore undergoes an asymmetric breathing during the 10 ns whereby S_A and S_D move outward and S_B and S_E inward. Accompanying these translations are small rotations. S_A and S_C twist clockwise and S_B and S_E counterclockwise. Such subunit motion could plausibly be transmitted directly to the transmembrane helices forming the ion channel. The sizes of these motions are no larger than 1 Å, but an effect this size, when transmitted to the transmembrane region, may be sufficient to alter ion flow in the narrow pore. Similar rotations for the inner β-sheets of muscle α-subunits have been observed in electron microscopy structures (Unwin et al., 2002). In this case, the sheets are also seen to rotate counterclockwise going from the activated to the activatable state. To test if this type of sheet motion was detectable in the simulations, a similar analysis was performed on partitions of the subunits into inner and outer β-strands. However, the translational and rotational motions of the inner and outer strands were found to behave similarly to their respective subunits, implying that the subunits remain fairly rigid during the simulation.

The other type of motion observed here that would connect with the transmembrane region is the change in the Cys loop seen in S_B. This subunit happens to be one that moves inward and counterclockwise. Such motions may encourage the displacement of the loop in this direction. The formation of a salt bridge between R132 on the Cys loop and E44 would also stabilize this motion. Salt bridges involving the Cys loop are particularly noteworthy because of their proximity to the transmembrane region. In the $GABA_A$ α-subunit, a variable pattern in the formation of salt bridges between K279 in the M2-M3 linker region and D57 or D149 has been observed depending on GABA concentration (Kash et al., 2003). It was found that the K279-D149 salt bridge only forms in the presence of high GABA concentration, whereas the K279-D57 bridge forms independently of GABA. A slightly different salt bridge pattern may arise for α7 with R132 choosing between E44 and possibly D265 in the M2-M3 linker region. If the R132-E44 salt bridge, characteristic of the activatable state, is preferred by S_B, then this is further evidence that S_B is moving toward the activatable state.

Some interesting relationships may be seen between the binding site motions and the subunit motions. The relative motion of the subunits is matched by backbone motions of residues in three of the binding sites, I_{AB}, I_{BC}, and I_{DE}. I_{AB} and I_{DE} experience an outward shear of the plus subunit. At I_{BC} both subunits move inward together. However, the binding-site residues at I_{CD} and I_{EA}, expected to have an outward shear of the minus subunit, compress slightly but largely move together, outward in the case of I_{CD} and counterclockwise for I_{EA}. Another characteristic of these two binding sites is that loop C moves inward much less because the minus subunit, with which loop C has contact, moves outward. Overall, backbone motion of the binding site residues parallels subunit motion to a large extent. More intriguing are the differences that arise at each interface. There is an interesting correlation between the W54 and L118 side chains and the subunit motions. At I_{BC} and I_{EA}, for which χ_1 of L118 begins as *gauche+*, pointing more into the binding site, W54 also adopts a *gauche+* orientation and also swings into the binding site. At the same time, S_B and S_E move inward and rotate counterclockwise. However, at I_{AB} and I_{DE}, for which χ_1 of L118 begins as *trans*, then W54 moves into the *gauche−* conformation, swinging away from the binding site. This time, S_A and S_D move outward, S_A rotates clockwise whereas S_D experiences no net rotation. I_{CD} is less clear-cut but resembles I_{AB} and I_{DE}. How these subunit and binding-site motions are connected remains subtle. It appears that when these two side chains point toward the binding site, there is a greater tendency for the interface to be tighter and the plus subunit to be drawn in. This pattern appears to repeat further down the interface at the Cys loop, which moves toward the minus interface at I_{BC}.

The asymmetry observed and its relationship with binding site structure have implications for ACh binding and the evolution of receptors themselves. The strength of binding would be expected to be different at each type of interface, some better and some worse. The more open interfaces, I_{AB} and I_{DE}, with W54 more favorably placed, would be expected to bind ACh more readily. Once they do bind, the interactions of ACh with the binding-site side chains may induce the plus subunits to drift back inward to a more symmetrical structure resembling AChBP. This would then improve the binding at the other interfaces, a possible mechanism of cooperativity. It may be that the binding of ACh in these two sites alone is sufficient for nAChR activation. That only two sites might be favorable for binding and, upon binding, necessary for activation, would be consistent with Hill coefficients for receptor activation by agonist no >2 observed for α7 (Corringer et al., 1995; Gopalakrishnan et al., 1995). On a possible relationship between the observed asymmetry and evolution, the asymmetry is reminiscent of inherently

asymmetrical nAChRs such as the neuronal $\alpha4\beta2$ and muscle $\alpha_2\beta\gamma\delta$ with respective subunit sequences $\alpha\beta\alpha\beta\beta$ and $\alpha\gamma\alpha\delta\beta$. These receptors contain two ACh-binding α-subunits separated by one non-ACh-binding subunit. In this simulation, S_A and S_D might play the role of the $\alpha4\beta2$ and muscle α-subunits based on the outward displacements they undergo in the relaxation compared with the electron microscopy structures of Unwin et al. (2002) and the supposedly more favorable interfaces I_{AB} and I_{DE} for ACh binding. It might also be argued that S_B and S_E resemble the α-subunits based on their counterclockwise rotations observed in the simulation and rotations in the same direction detected in the electron microscopy structures. Whereas this asymmetry may occur spontaneously for $\alpha7$, it appears to be enforced for the $\alpha4\beta2$ and muscle nAChRs by the different subunit compositions. Mutations in nAChR subunits away from α-subunits may have been tolerated as long as they preserved this capability of asymmetry.

CONCLUSION

A 10-ns molecular dynamics simulation of a homology model of the $\alpha7$ LBD has demonstrated its stability. In addition, it has also revealed some of the motions that take place in the LBD and suggested how ligand binding correlates with larger-scale subunit motions that would connect with the transmembrane region. In particular, conformational changes in the side chains of W148, W54, and L118 have been correlated with larger subunit motions in the LBD and motion of the Cys loop in S_B. The resulting structure may more closely resemble the activatable state, and the asymmetry with binding sites of different affinity for ACh may be a natural property of $\alpha7$. These interpretations are speculative and require closer examination, as the short 10-ns simulation time would have sampled only a portion of the repertoire of motions available to the LBD, and the simultaneity of motions may be coincidental. There is also an element of uncertainty as to how representative the motions are, given the use of a homology model. Having a full crystal structure and better simulation sampling methods would provide the ideal solution to addressing these deficiencies. In the meantime, we plan to undertake further simulations of the model with a range of bound ligands including agonists, antagonists, and potentiators, and with the lipid bilayer and most of the transmembrane domain present, now made possible by the recent electron microscopy transmembrane structure minus the vestibule region between the M3 and M4 helices (Miyazawa et al., 2003). These simulations should make clearer the causes and possible functional relevance of the different motions observed.

We thank Jung-Hsin Lin for helping with the molecular dynamics simulations; Jens Nielsen for assistance with pKa calculations; the Kollman group for providing an early version of AMBER 7; and Stewart Adcock, Richard Law, and Jessica Swanson for helpful discussions.

This work has been supported by grants from the National Science Foundation; the National Institutes of Health; the San Diego Supercomputer Center; National Biomedical Computation Resource at the University of California, San Diego; the Center for Theoretical Biological Physics; Accelrys; and the W. M. Keck Foundation.

REFERENCES

Adcock, C., G. R. Smith, and M. S. P. Sansom. 2000. The nicotinic acetylcholine receptor: from molecular model to single-channel conductance. *Eur. Biophys. J.* 29:29–37.

Arias, H. R. 1997. Topology of ligand binding sites on the nicotinic acetylcholine receptor. *Brain Res. Brain Res. Rev.* 25:133–191.

Berendsen, H. J. C., J. P. M. Postma, W. F. van Gunsteren, A. Di Nola, and J. R. Haak. 1984. Molecular dynamics with coupling to an external bath. *J. Chem. Phys.* 81:3684–3690.

Brejc, K., W. J. van Dijk, R. V. Klaassen, M. Schuurmans, J. van der Oost, A. B. Smit, and T. K. Sixma. 2001. Crystal structure of an ACh-binding protein reveals the ligand-binding domain of nicotinic receptors. *Nature.* 411:269–276.

Brooks, B. R., R. E. Bruccoleri, B. D. Olafson, D. J. States, S. Swaminathan, and M. Karplus. 1983. CHARMM: A program for macromolecular energy minimization and dynamics calculations. *J. Comp. Chem.* 4:187–217.

Changeux, J. P., and S. J. Edelstein. 1998. Allosteric receptors after 30 years. *Neuron.* 21:959–980.

Changeux, J. P., and S. J. Edelstein. 2001. Allosteric mechanisms in normal and pathological nicotinic acetylcholine receptors. *Curr. Opin. Neurobiol.* 11:369–377.

Corringer, P. J., J. L. Galzi, J. L. Eiselé, S. Bertrand, J. P. Changeux, and D. Bertrand. 1995. Identification of a new component of the agonist binding site of the nicotinic $\alpha7$ homooligomeric receptor. *J. Biol. Chem.* 270:11749–11752.

Corringer, P. J., N. Le Novère, and J. P. Changeux. 2000. Nicotinic receptors at the amino acid level. *Annu. Rev. Pharmacol. Toxicol.* 40:431–458.

Essmann, U., L. Perera, M. L. Berkowitz, T. Darden, H. Lee, and L. G. Pedersen. 1995. A smooth particle mesh Ewald method. *J. Chem. Phys.* 103:8577–8593.

Gasteiger, J., and M. Marsili. 1980. Iterative partial equalization of orbital electronegativity: a rapid access to atomic charges. *Tetrahedron.* 36:3219–3228.

Gillilan, R. E., and F. Wood. 1995. Visualization, virtual reality, and animation within the data flow model of computing. *Comput. Graphics.* 29:55–58.

Goodford, P. J. 1985. A computational procedure for determining energetically favorable binding sites on biologically important macromolecules. *J. Med. Chem.* 28:849–857.

Gopalakrishnan, M., B. Buisson, E. Touma, T. Giordano, J. E. Campbell, I. C. Hu, D. Donnely-Roberts, S. P. Arneric, D. Bertrand, and J. P. Sullivan. 1995. Stable expression and pharmacological properties of the human $\alpha7$ nicotinic acetylcholine-receptor. *Eur. J. Pharmacol.* 290:237–246.

Grutter, T., and J. P. Changeux. 2001. Nicotinic receptors in wonderland. *Trends Biochem. Sci.* 26:459–463.

Hogg, R. C., M. Raggenbass, and D. Bertrand. 2003. Nicotinic acetylcholine receptors: from structure to brain function. *Rev. Physiol. Biochem. Pharmacol.* 147:1–46.

Humphrey, W., A. Dalke, and K. Schulten. 1996. VMD: visual molecular dynamics. *J. Mol. Graph.* 14:33–38.

Jorgensen, W. L., J. Chandrasekhar, J. D. Madura, R. W. Impey, and M. L. Klein. 1983. Comparison of simple potential functions for simulating liquid water. *J. Chem. Phys.* 79:926–935.

Karlin, A. 2002. Emerging structure of the nicotinic acetylcholine receptors. *Nat. Rev. Neurosci.* 3:102–114.

Kash, T. L., A. Jenkins, J. C. Kelley, J. R. Trudell, and N. L. Harrison. 2003. Coupling of agonist binding to channel gating in the $GABA_A$ receptor. *Nature*. 421:272–275.

Laskowski, R. A., M. W. MacArthur, D. S. Moss, and J. M. Thornton. 1993. PROCHECK: a program to check the stereochemical quality of protein structures. *J. Appl. Crystallogr.* 26:283–291.

Le Novère, N., P. J. Corringer, and J. P. Changeux. 1999. Improved secondary structure predictions for a nicotinic receptor subunit: incorporation of solvent accessibility and experimental data into a two-dimensional representation. *Biophys. J.* 76:2329–2345.

Le Novère, N., T. Grutter, and J. P. Changeux. 2002. Models of the extracellular domain of the nicotinic receptors and of agonist- and Ca^{2+}-binding sites. *Proc. Natl. Acad. Sci. USA.* 99:3210–3215.

Merritt, E. A., and D. J. Bacon. 1997. Raster3D: photorealistic molecular graphics. *Method. Enzymol.* 277:505–524.

Miyazawa, A., Y. Fujiyoshi, M. Stowell, and N. Unwin. 1999. Nicotinic acetylcholine receptor at 4.6 Å resolution: transverse tunnels in the channel wall. *J. Mol. Biol.* 288:765–786.

Miyazawa, A., Y. Fujiyoshi, and N. Unwin. 2003. Structure and gating mechanism of the acetylcholine receptor pore. *Nature.* 423:949–955.

Molles, B. E., I. Tsigelny, P. D. Nguyen, S. X. Gao, S. M. Sine, and P. Taylor. 2002. Residues in the ε subunit of the nicotinic acetylcholine receptor interact to confer selectivity of Waglerin-1 for the α-ε subunit interface site. *Biochemistry.* 41:7895–7906.

Montal, M., and S. J. Opella. 2002. The structure of the M2 channel-lining segment from the nicotinic acetylcholine receptor. *Biochim. Biophys. Acta.* 1565:287–293.

Morreale, A., F. Maseras, I. Iriepa, and E. Gálvez. 2002. Ligand-receptor interaction at the neural nicotinic acetylcholine binding site: a theoretical model. *J. Mol. Graph.* 21:111–118.

Morris, G. M., D. S. Goodsell, R. S. Halliday, R. Huey, W. E. Hart, R. K. Belew, and A. J. Olson. 1998. Automated docking using a Lamarckian genetic algorithm and an empirical binding free energy function. *J. Comput. Chem.* 19:1639–1662.

Ortells, M. O. 1997. Prediction of the secondary structure of the nicotinic acetylcholine receptor nontransmembrane regions. *Proteins.* 29:391–398.

Ortells, M. O., G. E. Barrantes, C. Wood, G. G. Lunt, and F. J. Barrantes. 1997. Molecular modelling of the nicotinic acetylcholine receptor transmembrane region in the open state. *Protein Eng.* 10:511–517.

Pearlman, D. A., D. A. Case, J. W. Caldwell, W. S. Ross, T. E. Cheatham III, S. DeBolt, D. Ferguson, G. Seibel, and P. Kollman. 1995. AMBER, a package of computer programs for applying molecular mechanics, normal mode analysis, molecular dynamics and free energy calculations to simulate the structural and energetic properties of molecules. *Comput. Phys. Commun.* 91:1–41.

Ryckaert, J.-P., G. Ciccotti, and H. J. C. Berendsen. 1977. Numerical integration of the Cartesian equations of motion of a system with constraints: molecular dynamics of *n*-alkanes. *J. Comput. Phys.* 23:327–341.

Šali, A., and T. L. Blundell. 1993. Comparative protein modeling by satisfaction of spatial restraints. *J. Mol. Biol.* 234:779–815.

Schapira, M., R. Abagyan, and M. Totrov. 2002. Structural model of nicotinic acetylcholine receptor isotypes bound to acetylcholine and nicotine. *BMC Struct. Biol.* 2:1.

Sine, S. M. 2002. The nicotinic receptor ligand binding domain. *J. Neurobiol.* 53:431–446.

Sine, S. M., P. Quiram, F. Papanikolaou, H. J. Kreienkamp, and P. Taylor. 1994. Conserved tyrosines in the α subunit of the nicotinic acetylcholine receptor stabilize quaternary ammonium groups of agonists and curariform antagonists. *J. Biol. Chem.* 269:8808–8816.

Sine, S. M., H. L. Wang, and N. Bren. 2002. Lysine scanning mutagenesis delineates structural model of the nicotinic receptor ligand binding domain. *J. Biol. Chem.* 277:29210–29223.

Smit, A. B., N. I. Syed, D. Schaap, J. van Minnen, J. Klumperman, K. S. Kits, H. Lodder, R. C. van der Schors, R. van Elk, B. Sorgedrager, K. Brejc, T. K. Sixma, and W. P. M. Geraerts. 2001. A glia-derived acetylcholine-binding protein that modulates synaptic transmission. *Nature.* 411:261–268.

Tikhonov, D. B., and B. S. Zhorov. 1998. Kinked-helices model of the nicotinic acetylcholine receptor ion channel and its complexes with blockers: simulation by the Monte Carlo minimization method. *Biophys. J.* 74:242–255.

Unwin, N., A. Miyazawa, J. Li, and Y. Fujiyoshi. 2002. Activation of the nicotinic acetylcholine receptor involves a switch in conformation of the α subunits. *J. Mol. Biol.* 319:1165–1176.

Vriend, G. 1990. WHAT IF: a molecular modeling and drug design program. *J. Mol. Graph.* 8:52–56.

Wang, J. M., P. Cieplak, and P. A. Kollman. 2000. How well does a restrained electrostatic potential (RESP) model perform in calculating conformational energies of organic and biological molecules? *J. Comput. Chem.* 21:1049–1074.

Zhong, W. G., J. P. Gallivan, Y. Zhang, L. Li, H. A. Lester, and D. A. Dougherty. 1998. From ab initio quantum mechanics to molecular neurobiology: a cation-π binding site in the nicotinic receptor. *Proc. Natl. Acad. Sci. USA.* 95:12088–12093.